Thermodynamic Selectivity and Kinetic Control in the Encapsulation of Spiropyran Derivatives by Cucurbit[8]uril

Yinghui Niu,[†,‡] Fengbiao Chen,[†,‡] Xinru Guo,[†] Yinjun Chen,[*,†] Jin Wen,[*,†] and Meifang Zhu[†]

†*State Key Laboratory of Advanced Fiber Materials, College of Materials Science and Engineering, Donghua University, Shanghai 201620, China*

‡*These authors contributed equally.*

E-mail: yj.chen@dhu.edu.cn; jinwen@dhu.edu.cn

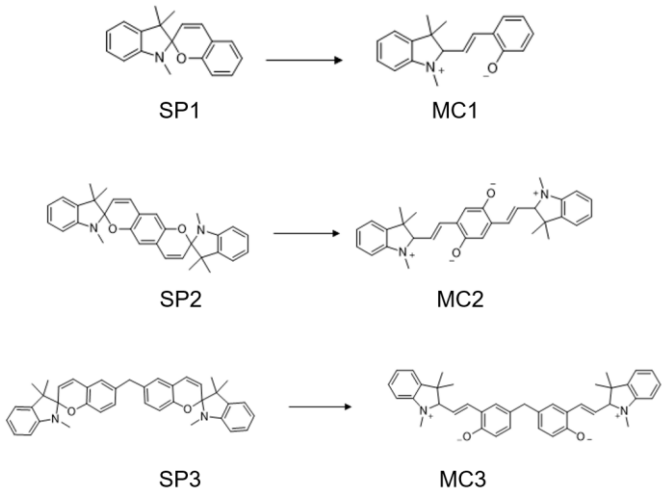

Figure S1. The molecular structural formulas of SP1-3 and MC1-3.

HR-ESI-MS (positive mode, m/z): a dominant peak at 665.2456 was observed, corresponding to the doubly protonated molecular ion $[M+2H]^{2+}$ of CB[8].

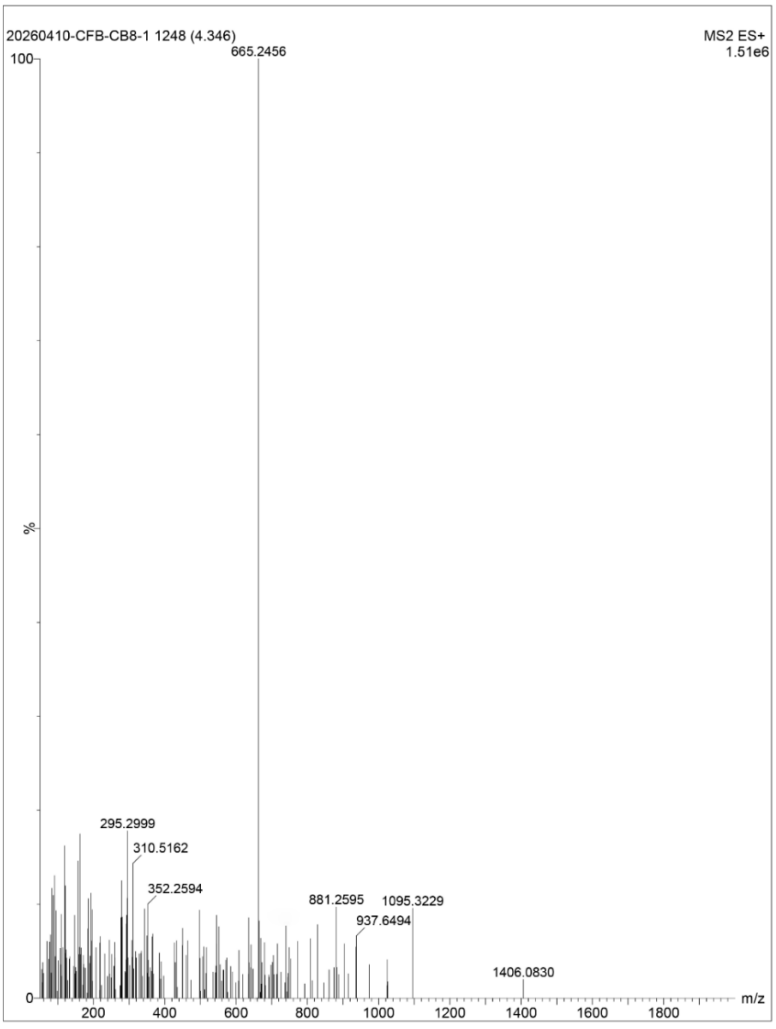

Figure S2. MS spectra of compound CB[8].

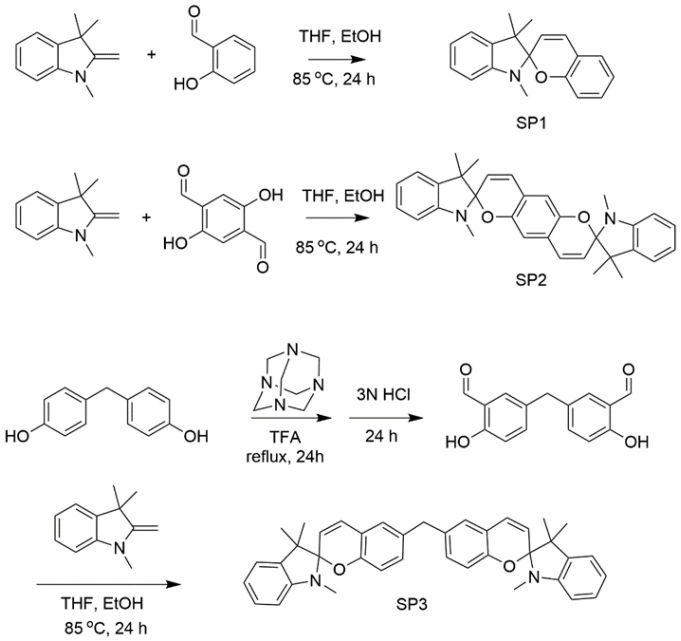

Figure S3. Synthesis route of spiropyran derivatives SP1-3.

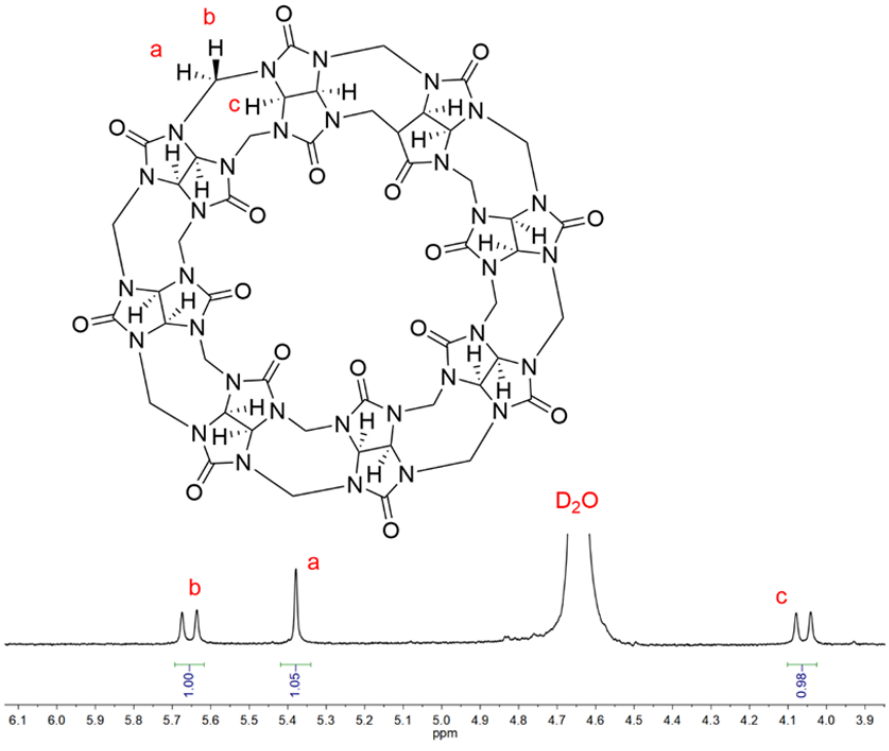

Figure S4. ^{1}H NMR spectrum of CB[8].

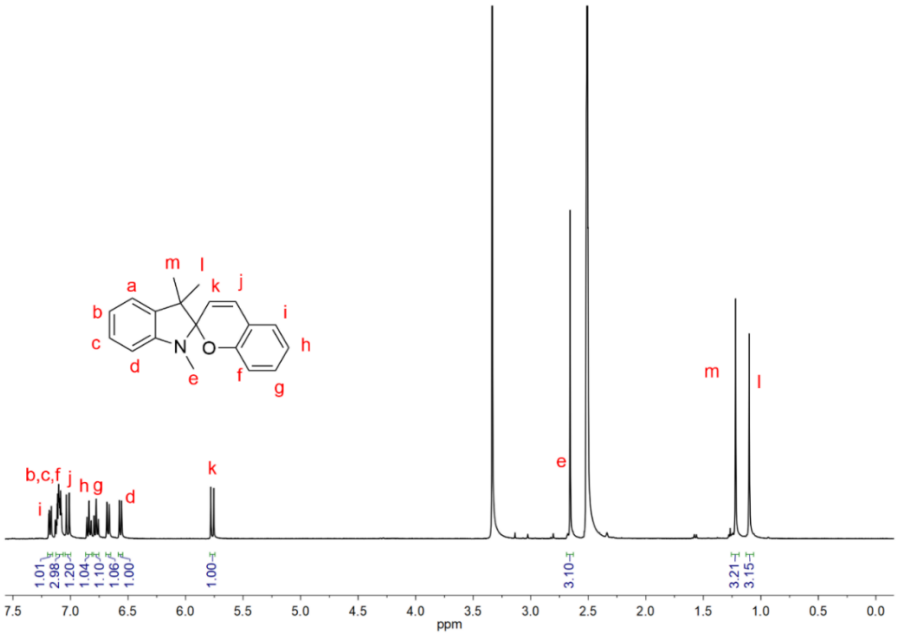

Figure S5. ^{1}H NMR spectrum of SP1. ^{1}H NMR (400 MHz, DMSO-d$_6$) δ 7.18 (dd, = 7.5, 1.7 Hz, 1H), 7.10 (ddt, J = 7.4, 3.5, 1.6 Hz, 3H), 7.02 (d, J = 10.1 Hz, 1H), 6.84 (td, J = 7.4, 1.1 Hz, 1H), 6.78 (td, J = 7.4, 1.0 Hz, 1H), 6.67 (d, J = 8.1 Hz, 1H), 6.57(d, J = 7.7 Hz, 1H), 5.77 (d, J = 10.2 Hz, 1H), 2.66 (s, 3H), 1.22 (s, 3H), 1.10 (s, 3H).

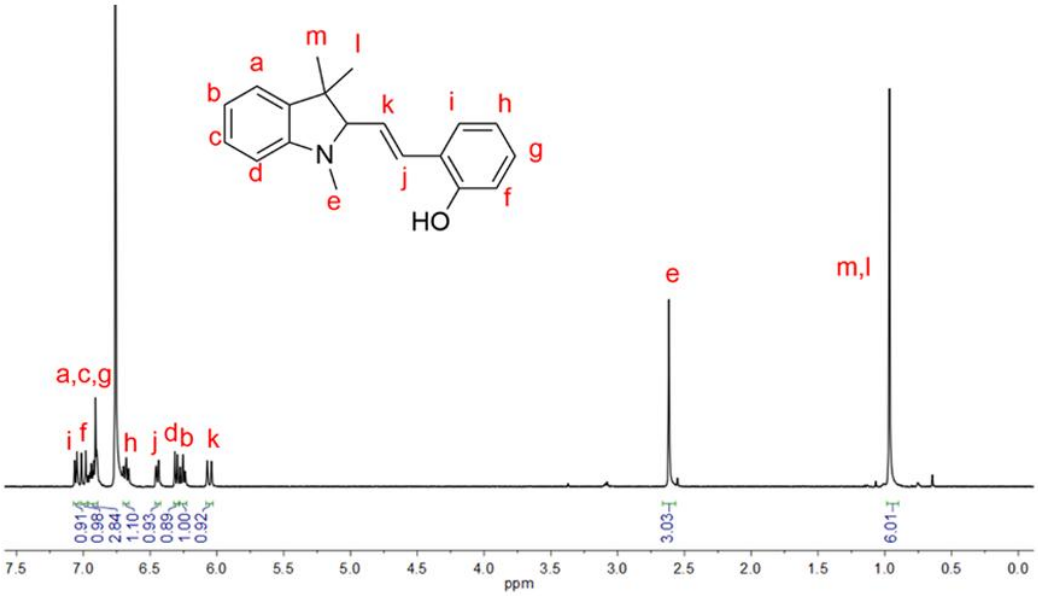

Figure S6. ^{1}H NMR spectrum of MC1. ^{1}H NMR (400 MHz, Deuterium Oxide) δ 7.07 7.03 (m, 1H), 7.00 (d, J = 12.7 Hz, 1H), 6.96–6.89 (m, 3H), 6.68 (t, J = 6.9 Hz, 1H), 6.46–6.42 (m, 1H), 6.30 (d, J = 8.1 Hz, 1H), 6.25 (t, J = 7.5 Hz, 1H), 6.06 (d, J = 12.7 Hz, 1H), 2.62 (s, 3H), 0.97 (s, 6H).

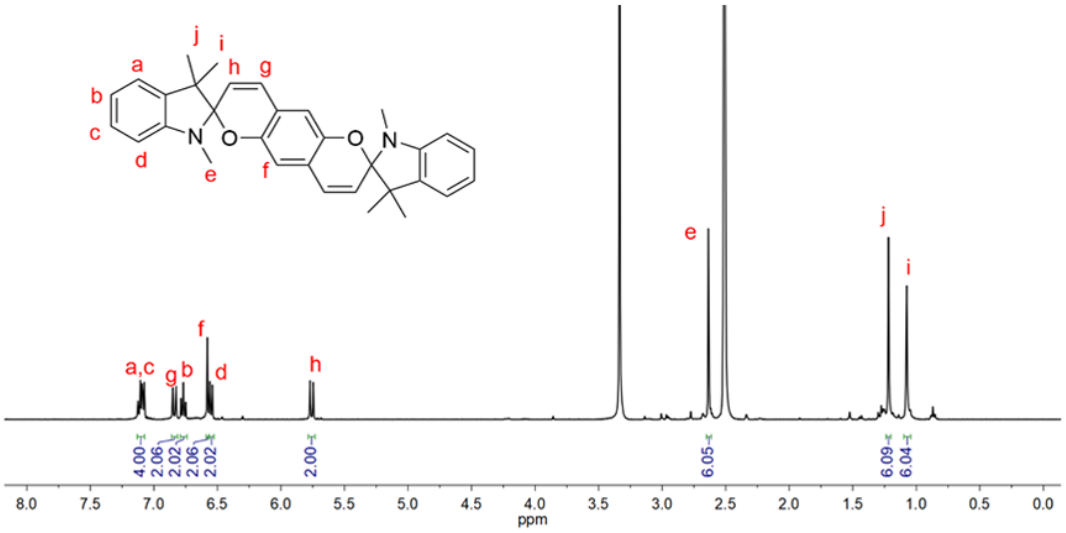

Figure S7. ^{1}H NMR spectrum of SP2. ^{1}H NMR (400 MHz, DMSO-d_6) δ 7.10 (td, J = 7.4, 5.5 Hz, 4H), 6.84 (d, J = 10.1 Hz, 2H), 6.77 (t, J = 7.4 Hz, 2H), 6.58 (s, 2H), 6.55 (d, J = 7.7 Hz, 2H), 5.76 (d, J = 10.2 Hz, 2H), 2.64 (d, J = 1.4 Hz, 6H), 1.22 (s, 6H), 1.08 (s, 6H).

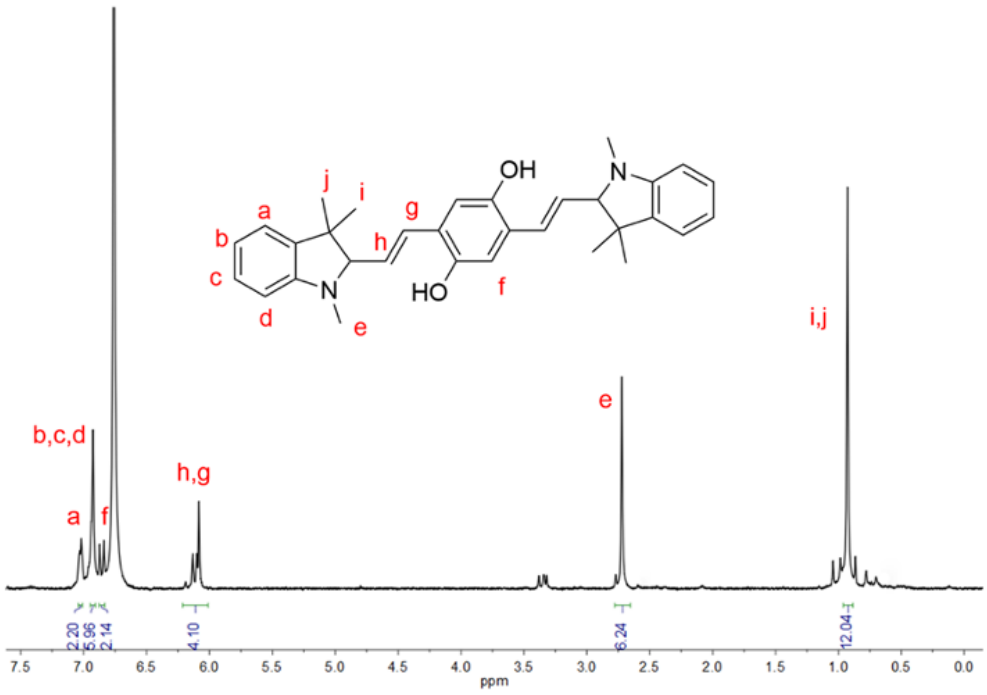

Figure S8. ^{1}H NMR spectrum of MC2. ^{1}H NMR (400 MHz, Deuterium Oxide) δ 7.03 (d, J = 5.8 Hz, 2H), 6.93 (m, J = 4.7 Hz, 6H), 6.86 (d, J = 12.8 Hz, 2H), 6.21–6.01 (m, 4H), 2.72 (s, 6H), 0.93 (s, 12H).

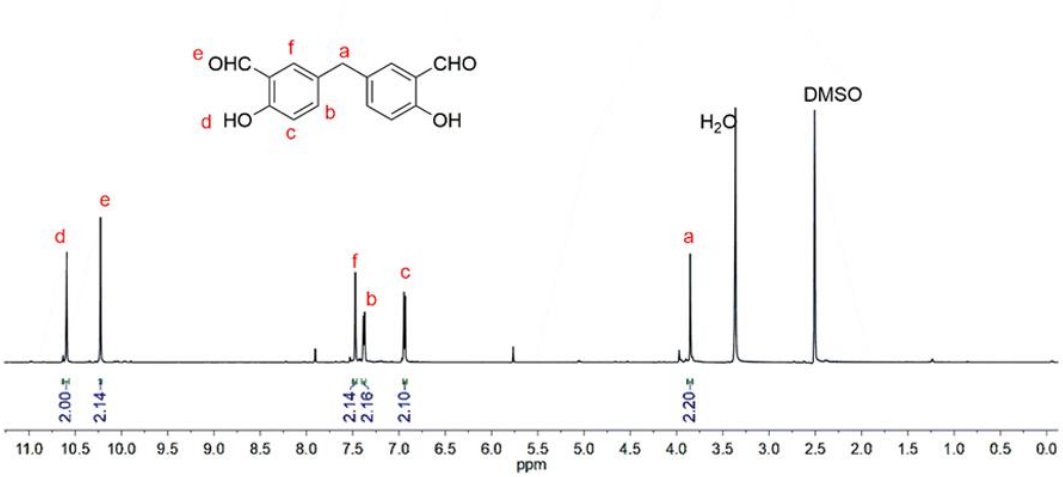

Figure S9. ^{1}H NMR spectrum of 5,5'-Methylenebis(2-hydroxybenzaldehyde). ^{1}H NMR (400 MHz, Chloroform-d) δ 10.85 (s, 1H), 9.77 (s, 1H), 7.30–7.24 (m, 2H), 6.88 (d, J = 8.4 Hz, 1H), 3.89 (s, 1H).

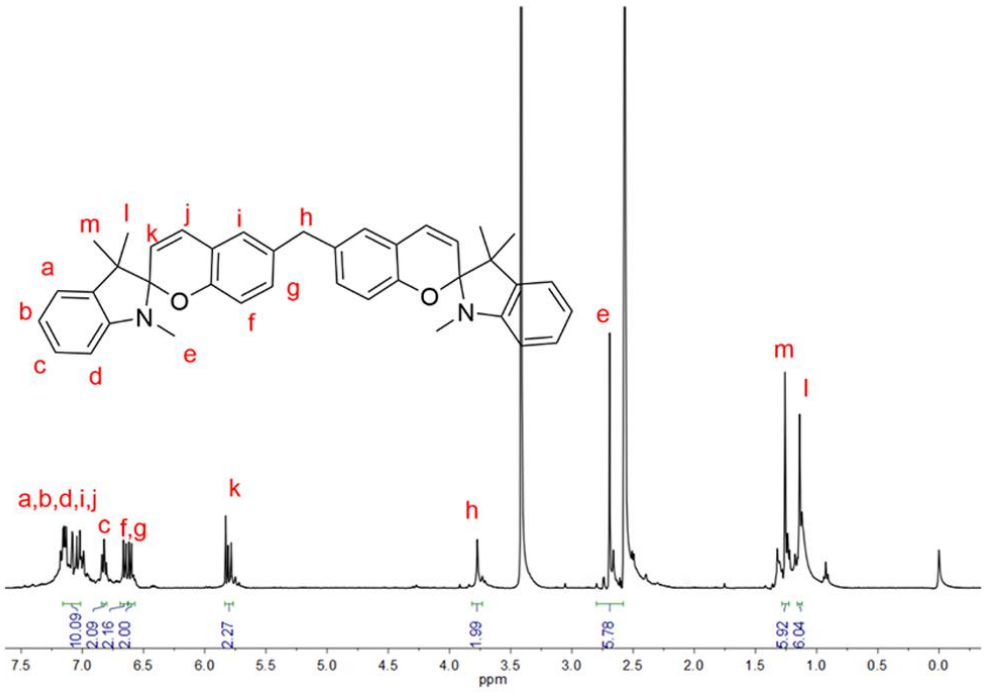

Figure S10. ^{1}H NMR spectrum of SP3. ^{1}H NMR (400 MHz, DMSO-d_6) δ 7.23–7.01 (m, 10H), 6.84–6.80 (t, 2H), 6.65 (d, J = 8.4 Hz, 2H), 6.61 (d, J = 7.7 Hz, 2H), 5.83–5.77 (m, 2H), 3.77 (s, 2H), 2.68 (s, 6H), 1.26 (s, 6H), 1.14 (s, 6H).

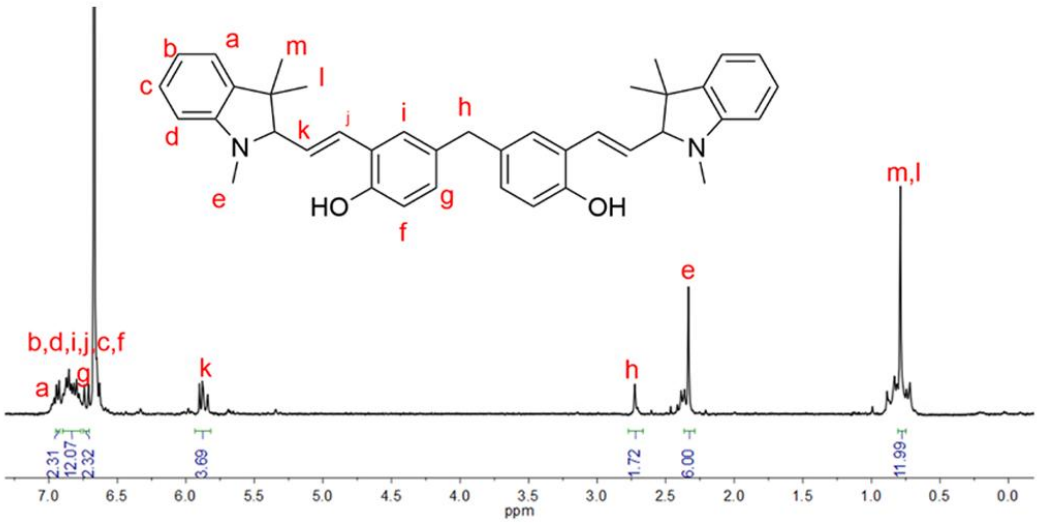

Figure S11. ^{1}H NMR spectrum of MC3. ^{1}H NMR (400 MHz, Deuterium Oxide) δ 6.93 (d, J =7.3 Hz, 2H), 6.99–6.77 (m, 12H), 6.73 (d, J = 12.3 Hz, 2H), 5.93–5.82 (d, 2H), 2.73 (s, 2H), 2.35 (s, 6H), 0.79 (s, 12H).

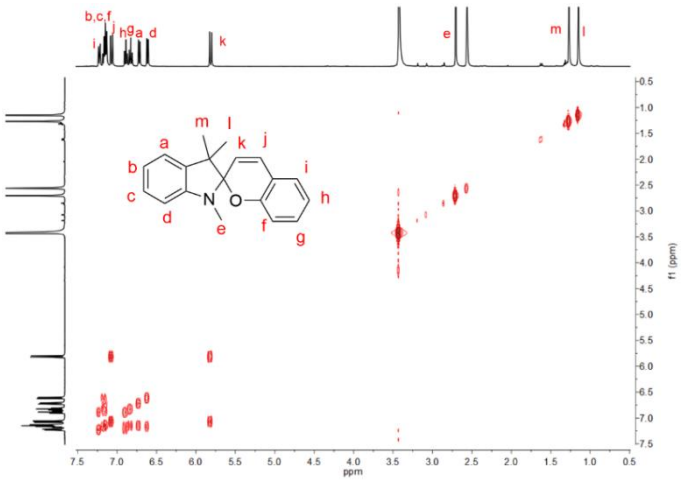

Figure S12. 2D ^{1}H-^{1}H COSY (400 MHz, DMSO-d_6) of SP1.

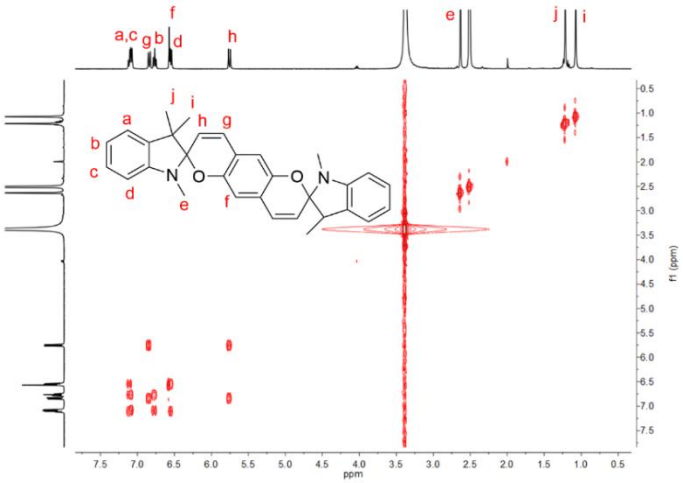

Figure S13. 2D ^{1}H-^{1}H COSY (400 MHz, DMSO-d_6) of SP2.

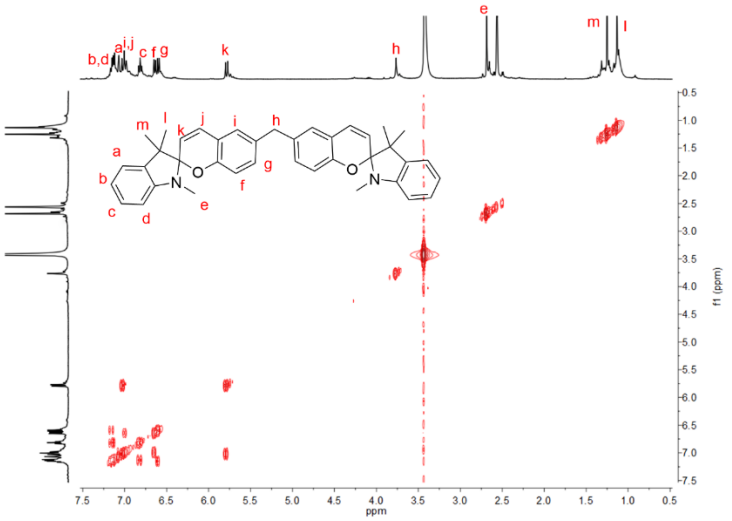

Figure S14. 2D ^{1}H-^{1}H COSY (400 MHz, DMSO-d_6) of SP3.

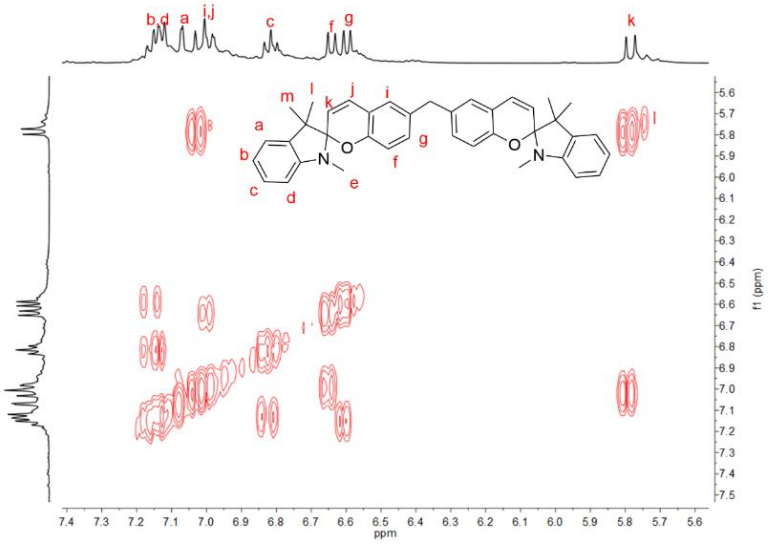

Figure S15. Two-dimensional COSY proton hydrogen assignment at the SP3 benzene ring position.

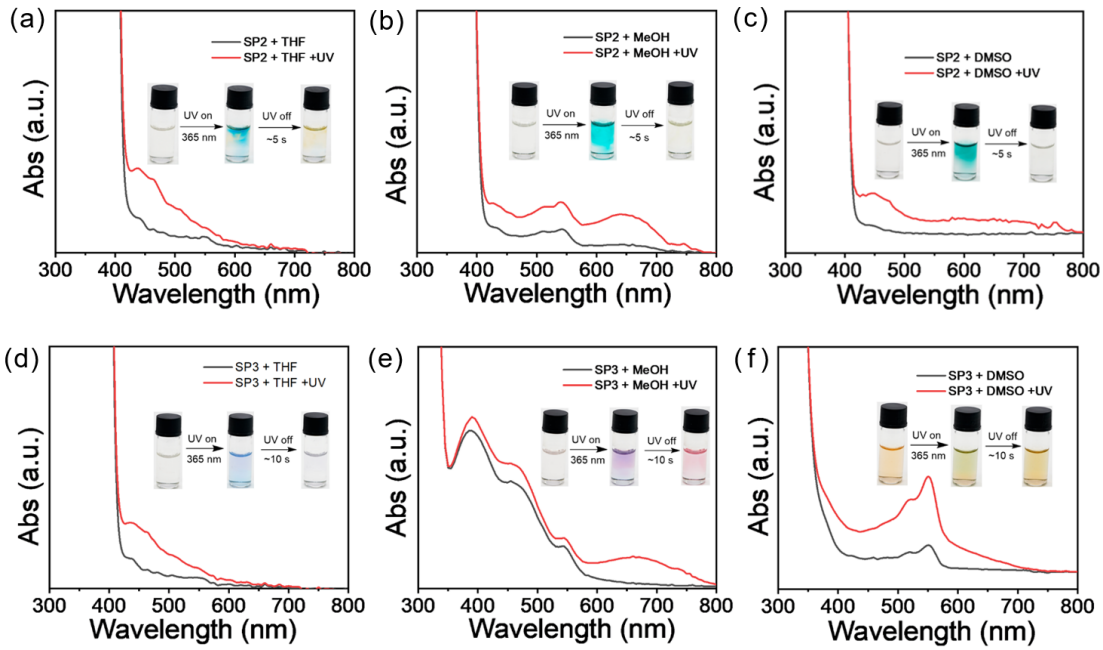

Figure S16. Photographs showing the color change and fade-back of SP2 and SP3 under 365 nm irradiation in THF, MeOH, and DMSO, and the corresponding UV-Vis absorption spectral changes. (a) SP2/THF; (b) SP2/MeOH; (c) SP2/DMSO; (d) SP3/THF; (e) SP3/MeOH; (f) SP3/DMSO.

Table S1. Key spectral positions and dipole moments for SP/MC species, together with the single-point energies of the corresponding guest@CB[8] complexes.

Guest	SP1	MC1	SP2	MC2	SP3	MC3
λ (nm)	350.0	455.0	389.5	521.3	349.2	452.4
μ (D)	1.46	5.66	0.001	0.36	1.98	7.70
E (hartree)	-5678.67	-5678.64	-6311.76	-6311.65	-6582.08	-6582.03

Notes: λ denotes the absorption maximum, and μ is the dipole moment in Debye (D).

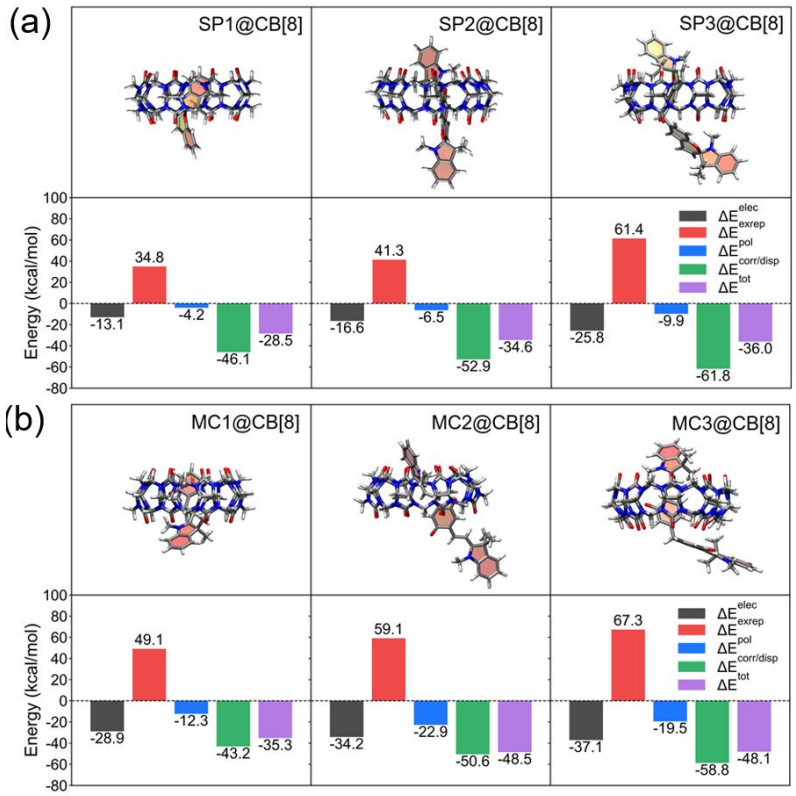

Figure S17. DFT-optimized geometries and GKS-EDA binding energy analyses of the host-guest inclusion complexes formed by CB[8] with (a) spiropyran isomers (SP1-3) and (b) merocyanine isomers (MC1-3). All calculations were performed at the ωB97X-D3/cc-pVDZ level.

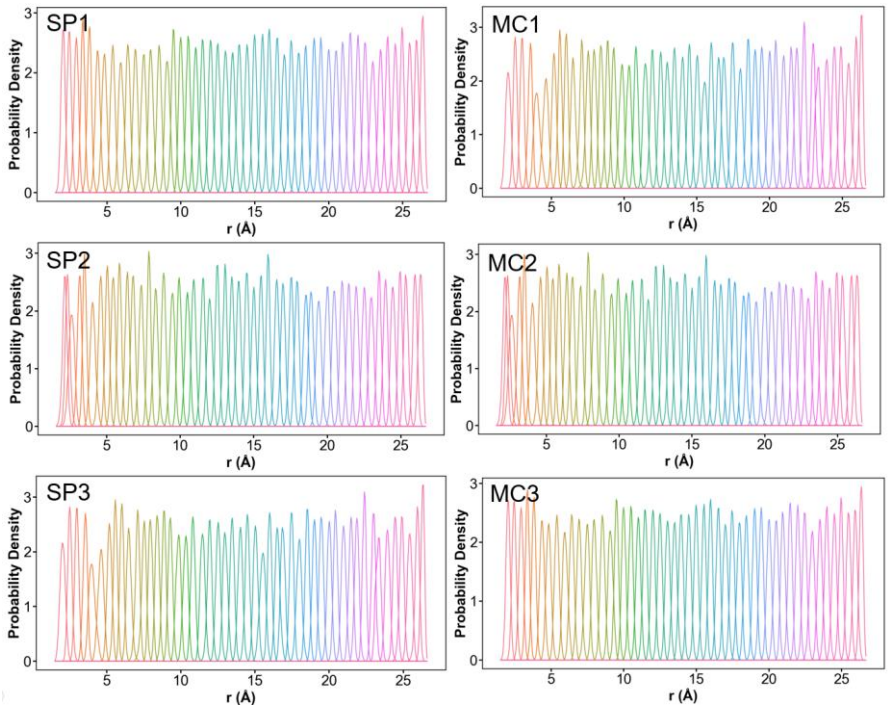

Figure S18. Probability density distributions of US windows for SP/MC@CB[8].

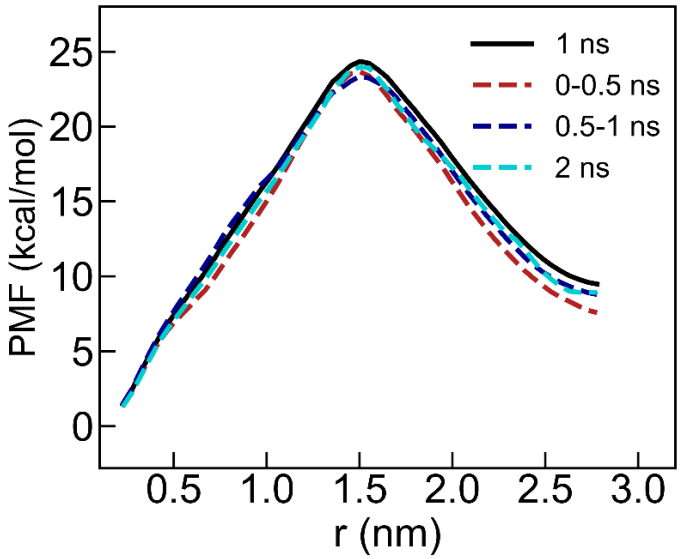

Figure S19. PMF convergence test for the SP1@CB[8] system. The PMF profiles were recon-structed from the original 1 ns trajectories of each um1brella window, the first 0-0.5 ns and second 0.5-1.0 ns segments, and the extended 2 ns sampling trajectories.

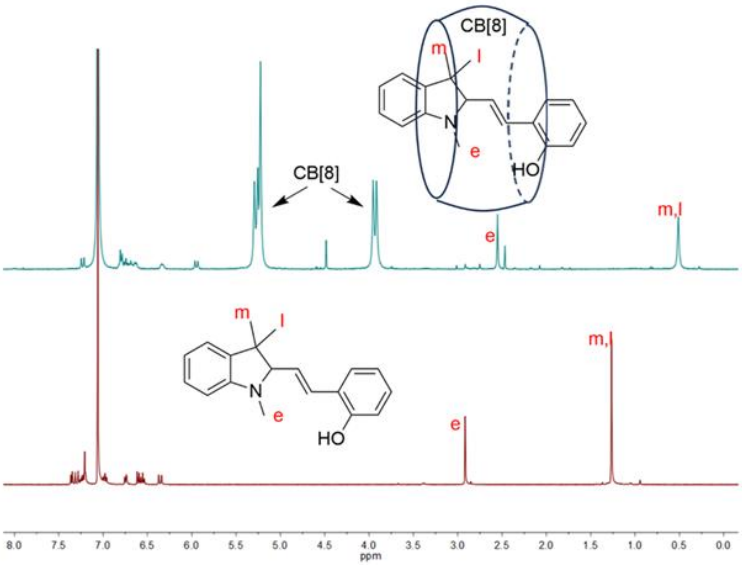

Figure S20. Comparison of NMR spectra of MC1 in 20% deuterium chloride in deuterium oxide solution before and after the addition of CB[8].

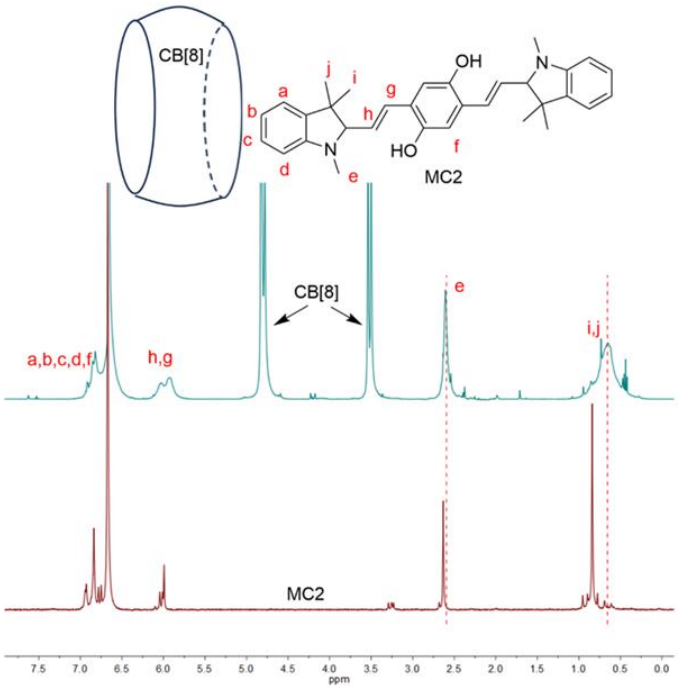

Figure S21. Comparison of NMR spectra of MC2 in 20% deuterium chloride in deuterium oxide solution before and after the addition of CB[8].

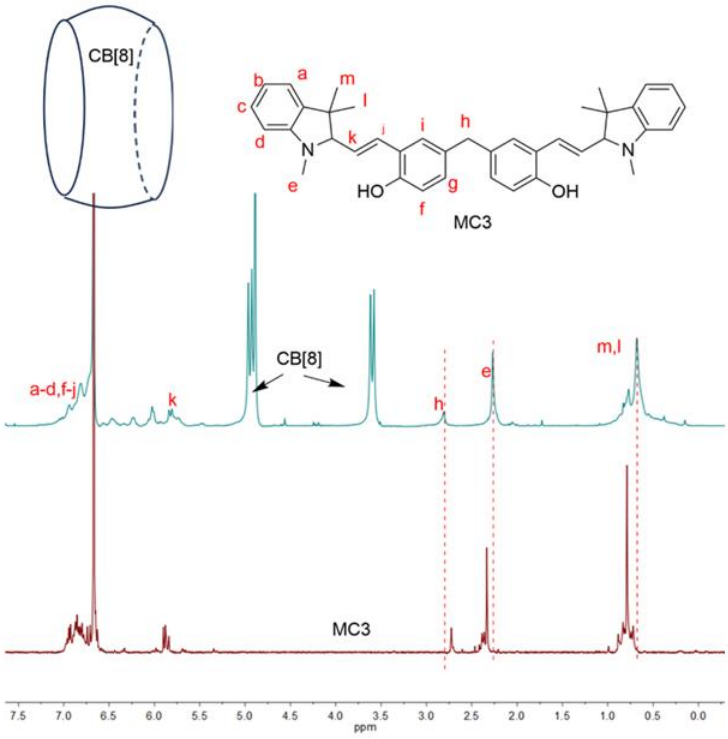

Figure S22. Comparison of NMR spectra of MC3 in 20% deuterium chloride in deuterium oxide solution before and after the addition of CB[8].

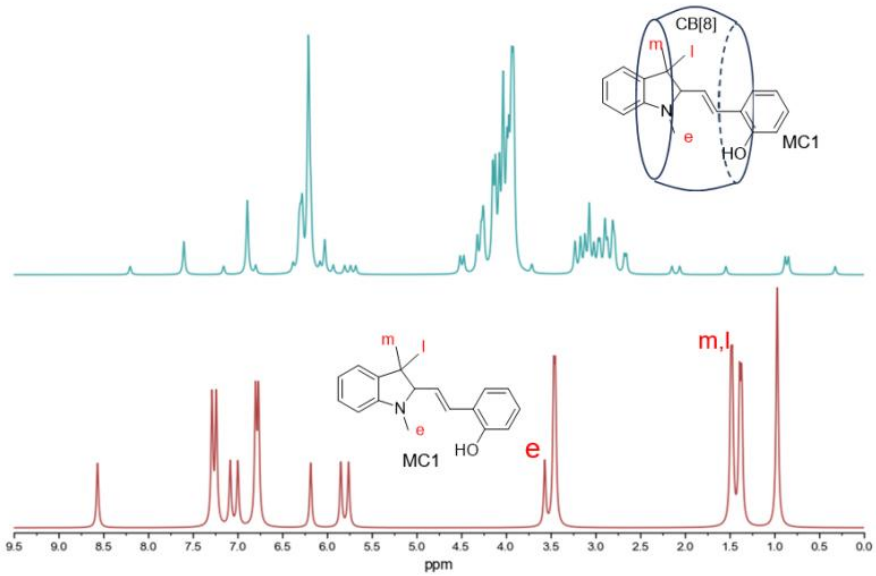

Figure S23. Comparison of simulated NMR spectra of MC1 before and after complexation with CB[8], calculated at the ωB97X-D3/cc-pVDZ level in the gas phase using TMS as the chemical shift reference.

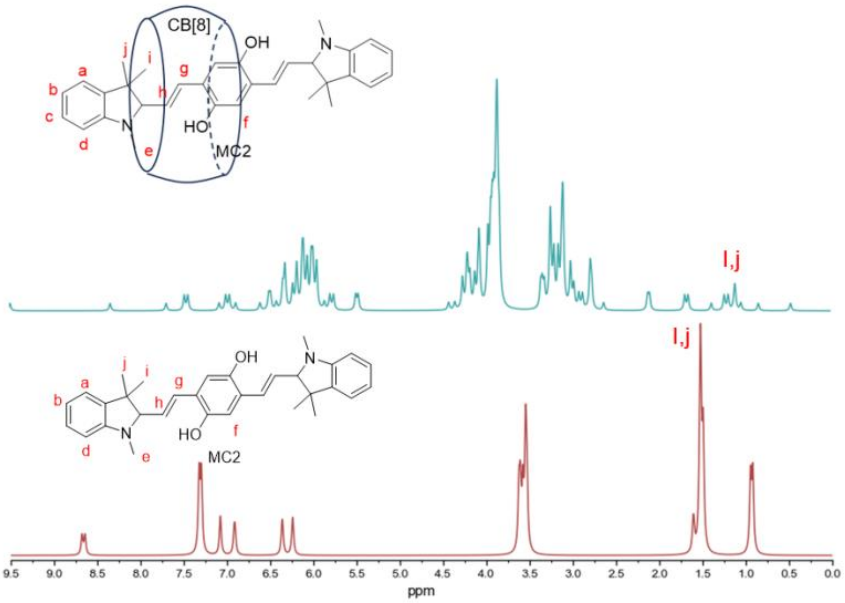

Figure S24. Comparison of simulated NMR spectra of MC2 before and after complexation with CB[8], calculated at the ωB97X-D3/cc-pVDZ level in the gas phase using TMS as the chemical shift reference.

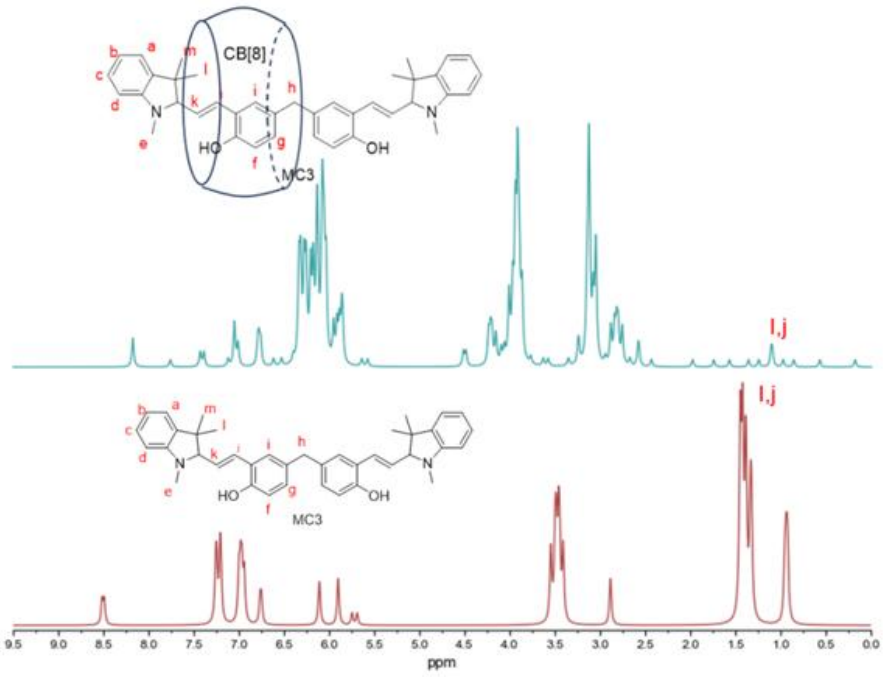

Figure S25. Comparison of simulated NMR spectra of MC3 before and after complexation with CB[8], calculated at the ωB97X-D3/cc-pVDZ level in the gas phase using TMS as the chemical shift reference.

TEA-dependent absorbance decay fitting analysis

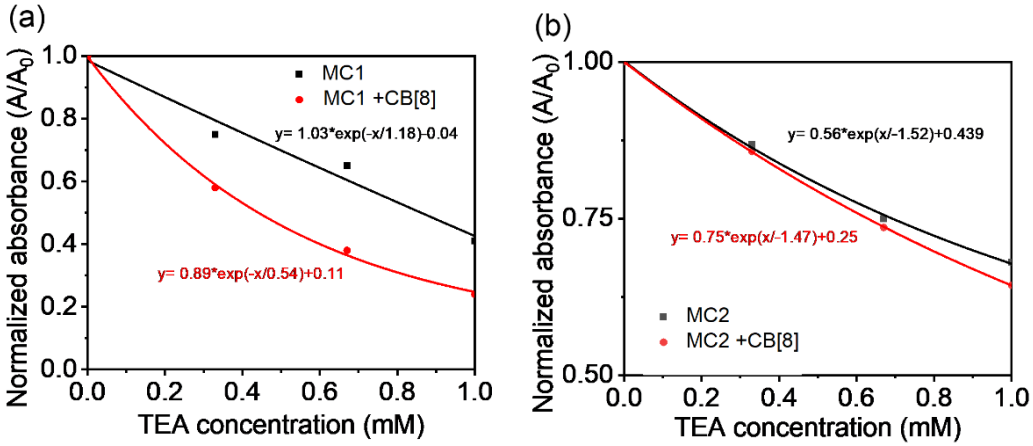

Figure S26. The normalized absorbance at equilibrium (or steady-state) as a function of TEA con-centration for different solutions: (a) MC1 and MC1 with CB[8]; (b) MC2 and MC2 with CB[8].

We have reanalyzed our dataset using a pseudo-first-order kinetic model based on the stepwise addition of TEA. The normalized absorbance at equilibrium (or steady-state) as a function of TEA concentration (shown in Fig. S26) can be described by an exponential decay function, which is characteristic of a first-order process influenced by a catalyst (TEA).

The general form of the fitted curve is:

$$A([\mathrm{TEA}]) = A_\infty + (A_0 - A_\infty) \cdot \exp\left(-\frac{[\mathrm{TEA}]}{K}\right)$$

Where $A([\mathrm{TEA}])$ is the normalized absorbance at a given TEA concentration, A_0 and $A_\infty$is the initial and final absorbance. Crucially, K is inversely related to the rate of the reaction: a smaller K value indicates a steeper decay and thus a faster reaction. For Fig. S26(a):

MC1 (black line): $y = 1.03 \cdot \exp(-x/1.18) - 0.04$

The apparent rate constant k_{obs}, MC1=1/1.18≈0.85 (in arbitrary units, since x is [TEA] in mM).

MC1 + CB[8] (red line): $y = 0.89 \cdot \exp(-x/0.54) + 0.11$

k_{obs}, MC1+CB[8]=1/0.54≈1.85.

The apparent kinetic constant K of the MC1–CB[8] complex is about 2.19 times smaller than that of free MC1 (1.85/0.85 ≈ 2.19), meaning the encapsulated guest reacts

approximately twice as fast at any point along the TEA titration. These quantitative findings strongly support a CB[8]-dependent kinetic acceleration.

Fig. S26(b) shows the quenching curves of MC2 with and without CB[8] upon stepwise addition of TEA. For MC2 (black line): k_{obs} (MC2) = 1/1.52 ≈ 0.66； For MC2+CB[8] (red line): k_{obs} (MC2+CB[8]) = 1/1.47 ≈ 0.68. Thus, the addition of CB[8] increases the apparent rate constant, indicating a certain degree of acceleration of the MC2 isomerization.

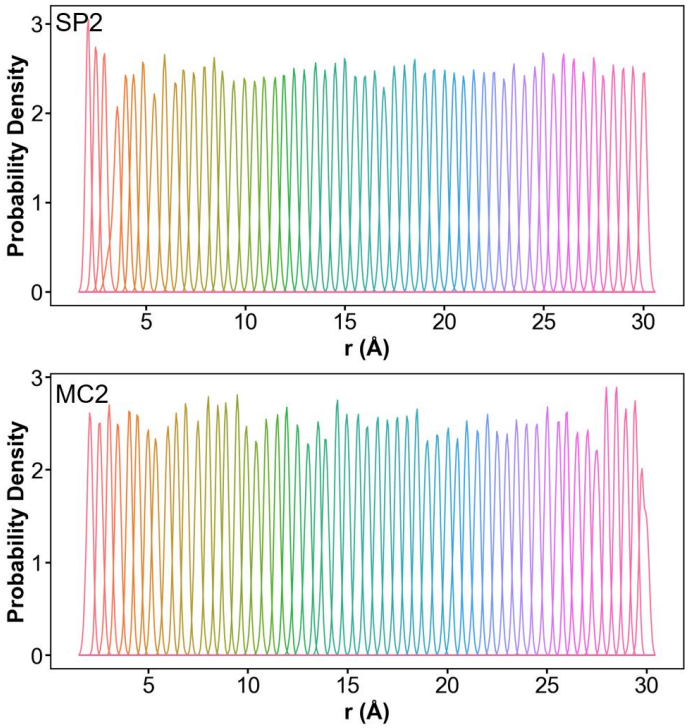

Figure S27. Probability density distributions of US windows for SP2/MC2@γ-CD.